Dynamics of a Periodically Forced Duffing Oscillator with Asymmetric Potential

Andrew Champion,[1] Ross Granowski,[2] Aemen Lodhi,[3] and Suchithra Ravi[4]

[1] *School of Computational Science and Engineering, Georgia Institute of Technology, Atlanta, Georgia 30332, USA*

[2] *School of Mathematics, Georgia Institute of Technology, Atlanta, Georgia 30332, USA*

[3] *School of Computer Science, Georgia Institute of Technology, Atlanta, Georgia 30332, USA*

[4] *School of Electrical and Computer Engineering, Georgia Institute of Technology, Atlanta, Georgia 30332, USA*

(Dated: December 14, 2012)

We compare a mechanically forced double-well Duffing oscillator with an asymmetric potential to numeric simulations of a symmetric potential system. Analysis is performed with time series data, phase portraits, recurrent Poincaré sections, attractor reconstruction from time delay embedding, and Lyapunov exponent estimation from this reconstruction. Our investigation finds that the asymmetric mechanical system can exhibit chaos while for the same forcing parameters symmetric simulation produces limit cycles above or below the chaotic threshold depending on the mechanical potential well used to estimate simulation parameters.

I. INTRODUCTION

The forced Duffing oscillator is a seminal system for the study of chaotic dynamics and development of analytical and experimental techniques for nonlinear systems. A common physical interpretation for the double-well case of the Duffing oscillator model considered here is a ferromagnetic beam positioned between two magnets while undergoing lateral forcing, as illustrated in Figure 1. This mechanical system elucidates several features of the model Duffing oscillator: a potential for the lateral position of the beam created by the two magnets; non-autonomous forcing resulting in motion of the beam, potentially chaotically between the two wells; and mechanical dissipation within the beam and from air resistance against the beam's motion.

Though the Duffing oscillator and the double-well beam system are simple and not of any obvious utility in their own right, they provide a structured model with few, well-

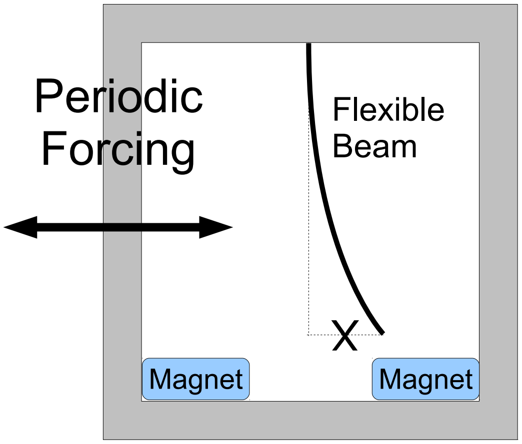

Figure 1. A common physical interpretation of the double well Duffing oscillator for $\alpha > 0$.

defined parameters and clear physical interpretations while still producing chaotic dynamics. This allows intuition into the system's behavior and creates an accessible and familiar setting for experimental design, data analysis, and diagnosis of unexpected results. All these features are valuable both for pedagogical purposes and for the development of new methods and tools for analysis, experimentation, computation, and diagnosis that may be extensible to more complex systems or other scientific or engineering applications.

Our original research question was the relation of dynamics of the Duffing oscillator to the form of the forcing function. Partial research goals towards investigating this question were to induce, record, analyze, and characterize chaotic dynamics in a mechanical double-well beam system. Parameters of the Duffing oscillator model are estimated from these experiments. Analysis of the experimental data was to be compared with analysis of simulation data. However, we observed asymmetry of the potential well in experiments with the double-well beam apparatus. Due to this asymmetry, for similar forcing the experimental apparatus exhibited chaotic dynamics while simulations with parameters estimated from the physical system did not.

A. The Duffing Equation

Duffing's eponymous model oscillator is governed by the nondimensional second-order ordinary differential equation[1]:

$$\ddot{x} + \delta\dot{x} - \alpha x + \beta x^3 = f\cos(\omega t) \qquad (1)$$

(note that in some literature α and β are interchanged and the sign of the x term is positive). The mechanical interpretation considered here for $\alpha > 0$ is principally due to Moon and Holmes[2]. Although the system is described in terms of $\mathbb{R}^2$ as $(x, y) = (x, \dot{x})$ and chaos is not possible in 2-dimensional systems, the non-autonomous forcing represented by $f\cos(\omega t)$ means (1) defines a vector field in 3-dimensional space, which enables chaos.

With no dissipation ($\delta = 0$) and no forcing ($f = 0$), the system is a true 2-dimensional

ODE:

$$\ddot{x} - \alpha x + \beta x^3 = 0 \tag{2}$$

For $\alpha < 0$ the system is single-well, with closed orbits around the center at the origin. With $\alpha > 0$, a double-well forms with a saddle node at the origin and centers at $\left(\pm\sqrt{\frac{\alpha}{\beta}}, 0\right)$. Homoclinic orbits extend from the origin around each of these centers, but otherwise trajectories are closed orbits as in the single well case. Initial conditions outside the homoclinic orbits will orbit around all three fixed points, i.e., around both wells, while those inside a homoclinic orbit remain in a single well.

In the beam system, this corresponds to an ideal beam without external forcing. The displacement of the tip of the beam is x and its velocity $\dot{x}$. If placed at any of the three fixed points the beam will remain there; perturb it slightly at either of the centers and it will oscillate near that magnet. Perturb the beam at the saddle node (equilibrium between the magnets) and it will enter an oscillation around one of the magnets. Start the beam with an initial condition large enough to place it outside of the homoclinic orbit and it will oscillate from one magnet to the other periodically. This physical interpretation can be formulated as a potential function derived from (2):

$$V(x) = \frac{\beta}{4}x^4 - \frac{\alpha}{2}x^2 \tag{3}$$

where all trajectories are curves of constant energy $E(x, \dot{x}) = \frac{1}{2}\dot{x}^2 + V(x)$.

With dissipation $\delta > 0$, the centers become spiral sinks (only the double-well, $\alpha > 0$ case will be considered for the remainder of this discussion; analogous results in the single-well case are trivial). Therefore all trajectories eventually spiral towards one of these fixed points, except for initial conditions at the origin and along stable manifolds of the saddle node situated there[3]. The physical interpretation from the undamped case extends intuitively with dissipation added; so long as the beam does not start at one of the three fixed points the amplitude of oscillations dissipates over time until it comes to rest at either of the sinks. The rate of energy change in the physical interpretation becomes

$$\frac{d}{dt}E = \dot{x}(\ddot{x} + \beta x^3 - \alpha x) = -\delta \dot{x}^2 \tag{4}$$

Since (4) is strictly negative for all cases where the beam is moving and not resting at a fixed point ($\dot{x} \neq 0$), energy is decreasing along all trajectories.

Adding forcing to counter this dissipation creates three cases of qualitative behavior determined by the magnitude of $f > 0$ and ω. To focus discussion here we consider ω constant. When f is small (heuristically $f\omega \sin(\omega t) \ll \delta$ and thus the absolute value of the integral of (4) is larger than energy added by forcing for all but small $|\dot{x}|$), the system is similar to the unforced damped case, except the spiral sinks are now stable limit cycles via a supercritical Hopf bifurcation at $f = 0$. In the beam system, the beam undergoes a dampening transient during which behavior is either similar to the damped, unforced case or is chaotic, before approaching the limit cycle oscillation in a single magnetic well. As f increases, the stable and unstable manifolds of the saddle node approach, then intersect at infinitely many points, creating chaotic behavior where trajectories escape one well and enter the other. As f increases further, the two limit cycles have merged into a single large limit cycle encompassing both wells. Beam behavior after the transient in this case is similar to the large $\dot{x}$ undamped, unforced case, except the oscillation of the beam approaches the limit cycle frequency and amplitude, rather than orbiting along a closed trajectory through its initial condition.

This qualitative description of the Duffing oscillator has assumed a symmetric double-well potential. Asymmetry of the potential wells in the mechanical system can result from asymmetric geometry of the magnet placement, differences in the magnetic field strength between the magnets, or curvature of the beam. As asymmetry affects the position of the fixed points, shape of orbits and limit cycles, and orientation of the manifolds it clearly impacts the onset of chaotic behavior. Methods of modeling and estimating such asymmetry have recently been proposed[4,5].

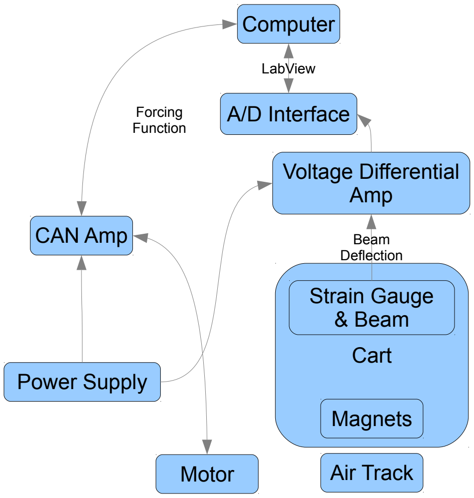

Figure 2. Logical organization and electrical connections of the experimental apparatus.

II. METHODS

A. Materials and Sensors

Our experimental apparatus for the double-well beam system was an inverted version of the system illustrated in Figure 1. Alternative implementations of the system effect forcing through variation of current in the electromagnets used for the potential wells, obviating the need for mechanical forcing of the entire system[6]. The organization and connection of the components of the apparatus is shown in Figure 2. The original planned apparatus was to have magnets or weights attached to the end of the beam in addition to using stationary electromagnets for the potential wells. Preliminary trials with a beam cut from steel shim stock found that attaching magnets at the end of the beam created undesired effects such as gravity-induced potential at the extremes of beam deflection and torsion around the axis of elongation of the beam. Using thicker stock to counter these effects increased the stiffness of the beam, requiring stronger magnets to achieve desired potentials. Instead, no magnets or weights were attached to the end of the beam and stronger rare-earth magnets were used for the potential wells instead of electromagnets. This would ultimately contribute to the observed potential well asymmetry, as permanent magnets can not be as readily calibrated as electromagnets.

Initial plans also included a high-speed camera to capture the motion of the beam to supplement data from a strain gauge attached at the base of the beam. This was due to concerns that the accuracy of strain gauges can drift over time and that the deflection of the beam may be nonlinear such that measurements at the gauge attachment point near the base were not sufficiently precise to resolve the position of the tip of the beam. However, the drift in accuracy of the strain gauge (which in our apparatus was principally due to drift in the voltage differential amplifier's potentiometer) was on a sufficiently slow timescale that it did not interfere with the timescale of our individual experimental recordings (most less than five minutes). Manual measurements of beam deflection and gauge voltage found it precise within the range of motion possible in the experimental apparatus. Within this range an approximately linear relationship between voltage and position was measured with a slope of $\approx 32.1 \frac{\mathrm{mm}}{\mathrm{V}}$.

Given the constraints of magnets available and range of motion of the forcing motor,

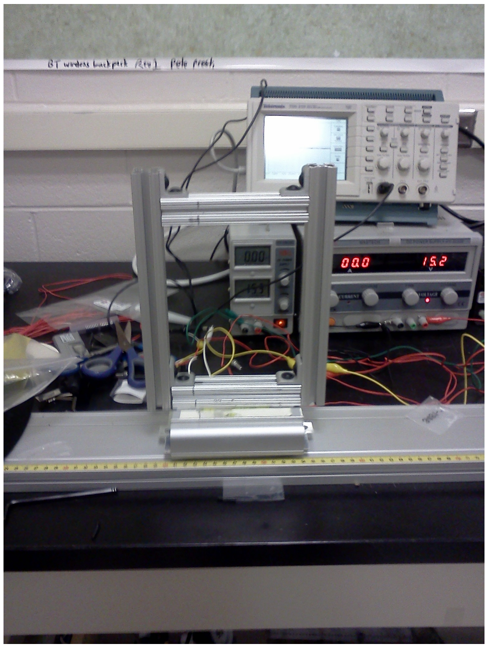

Figure 3. An early iteration of the experimental apparatus. A wheeled cart rests in a grooved aluminum track to be forced laterally by an arm extending from a fixed motor (not shown).

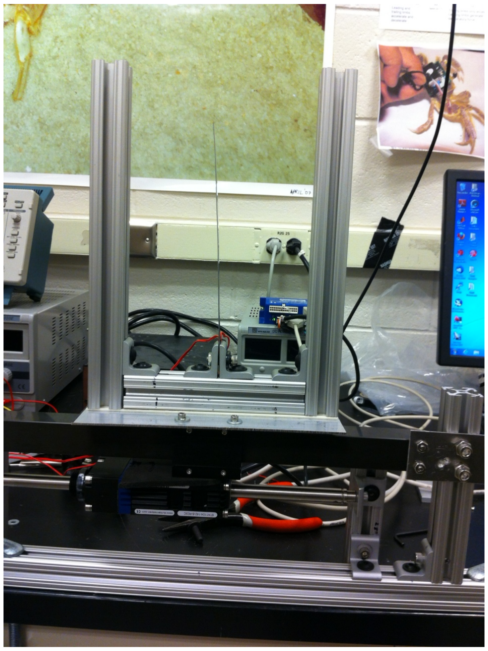

Figure 4. An improved experimental apparatus with the beam system mounted to an air track. The motor moves with the cart and is attached with adhesive. The magnets (not attached in this image) are suspended above the beam.

a shim stock 0.007 inches (1.778×10^{-4} m) thick was selected. The beam was clamped between two steel plates and heated to reduce curvature resulting from the fabrication process. Some curve remained in the beam, both around its axis of elongation and along the direction of lateral forcing of the system.

B. Forcing Apparatus

The initial chassis for the beam and magnets and apparatus for effecting forcing is shown in Figure 3. A wheeled cart running along an aluminum track was to be forced by an arm extending from a fixed motor. The frame supporting the magnets and beam mounts is constructed from 80/20 aluminum. Despite careful selection of the region of track to be used and lubrication of the cart's wheels, persistent problems with wheels binding and rough traversal of the track causing vibration necessitated a new apparatus.

To address these issues the cart and track were replaced with an air track consisting of a cart surrounding a well-machined square profile beam. Pressurized air forced between

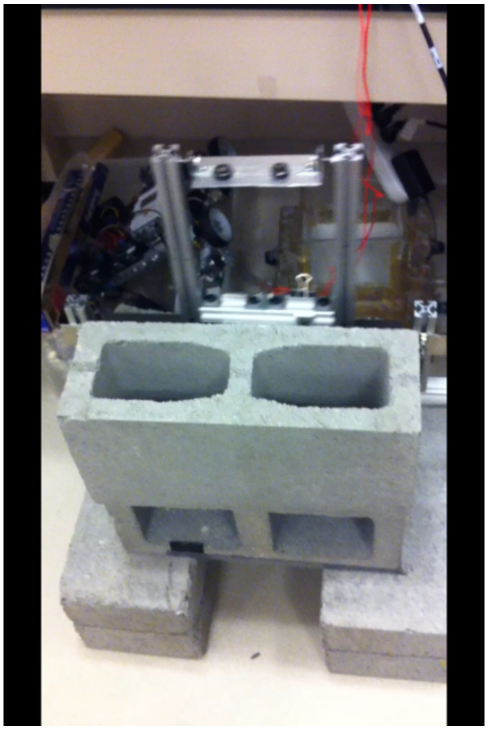

Figure 5. The final experimental apparatus attached to cinderblocks in motion. Secondary magnets holding the primary potential well magnets to the top frame member are visible.

the cart and track suspends the cart away from the track surface, reducing friction. A later iteration of this design than the one shown in Figure 4 connected the cart and motor securely with an aluminum bracket. Though friction had been reduced from the original design, the greater forcing magnitude achieved by this apparatus caused the beam to strike the 80/20 frame, and vibrations of the workbench on which the apparatus was mounted from the periodic forcing reciprocally acted on the system and influenced beam dynamics.

The final iteration of the apparatus, shown in Figure 5, resolved these issues by widening the 80/20 frame and mounting the entire system on cinderblocks adhered to each other and to the laboratory floor. The only vibration still present in the system is during strong forcing near the extremes of motion. Inertia can cause the air cart to torque on the track, inducing rotational vibration around the front-to-back axis of the system. A possible improvement to the system would reduce (and rotate, but not eliminate) this vibration by mounting the beam frame to the cart horizontally rather than vertically, with it offset such that the center of mass is centered and low over the cart. Another limitation of the maximum forcing magnitude of the apparatus is the heat and current limitations of the motors. 120mm fans cool both the motor and the CANbus amplifier controlling it. However, during repeated experimental trials heat accumulation in the amplifier can necessitate early termination of trials. With the 75V DC power supply used the apparatus can not reliably produce large f limit cycle forcing; chaotic f forcing can be produced for short trial intervals through careful calibration.

III. RESULTS

All voltage time series from the strain gauge were sampled at 10kHz and processed with a Butterworth filter with a 6kHz pass frequency to remove high-frequency noise. The longest chaotic trial of 4 minutes observed was sinusoidally forced at 4Hz with an amplitude of 2100 counts of the motor encoder, which at $0.006\frac{\text{mm}}{\text{count}}$ is 12.6mm. This corresponds to 0.392V by the strain gauge conversion factor. Our estimated forcing for this trial is $f \approx 6.272\frac{\text{V}}{\text{s}^2}$.

A. Parameter Estimation

Parameters are estimated from small f limit cycle experiments in each well using methods from Berger and Nunes Jr[6] for a symmetric potential beam oscillator. Data from these trials, such as that shown in Figure 6, was detrended to be stationary so sen-

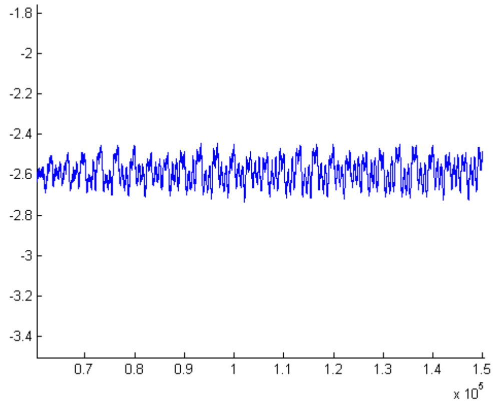

Figure 6. Measured voltage versus time (in 0.1ms) for a run with small f limit cycle behavior.

sor drift would not affect estimation of fixed points and limit cycles. Estimation of limit cycles from this data matched unforced placement of the beam in each potential well, with the stable points near $\pm\sqrt{\frac{\alpha}{\beta}} \approx \pm 0.7\text{V} \approx \pm 22.5\text{mm}$. By ignoring forcing terms in (1), frequencies of simple harmonic motion can be estimated as

$$\omega_1 = \sqrt{2\alpha(1-\delta^2/8\alpha)} \tag{5}$$

$$\delta = \sqrt{8\alpha(1-\omega_1^2/2\alpha)} \tag{6}$$

$$\omega_0 = \sqrt{2\alpha} \tag{7}$$

where α is heuristically fit such that $\omega_0 = \omega_1 + \epsilon$.

Parameters were estimated for the left well from a small f limit cycle time series such that $\omega_{1,\text{left}} = 2.0\text{Hz}$, $\beta = \frac{\alpha}{.49}$ and $\delta = \sqrt{8\alpha(1-2/\alpha)}$. Choosing $\alpha = 2.01$ yields $\omega_0 = 2.004$, which is slightly larger than ω_1 as required. As detailed in Table I, this estimation process was repeated for the right well and for an average potential.

B. Time Series Analysis

A portion of the experimental strain gauge voltage time series from the aforementioned chaotic 2100 count, 4Hz run is shown in Figure 7. This data is not adjusted for gauge drift, so the magnetic wells are near -0.4V and $-1.8V$, a separation of 1.4V as expected from the fixed point calculation above. The beam can be observed hopping in a unpredictable fashion from one well to the other.

After filtering, $\dot{x}$ was estimated from this time series by numerical differentiation using the pairwise difference of sequential voltage values. With the first order derivate phase portraits could be plotted, including the one for this time series in Figure 8. Here the asymmetric potential wells are evident. Analysis of the Poincaré section shown in Figure 9 of the system requires more careful inspection. Coloring according to sequence of intersection with the plane helps reveal an

Table I. Estimated Duffing Model Parameters

Well	ω_1 (Hz)	α	ω_0 (Hz)
Left	2.00	2.01	2.0040
Right	4.76	11.33	4.7602
Average	3.38	5.71	3.3805

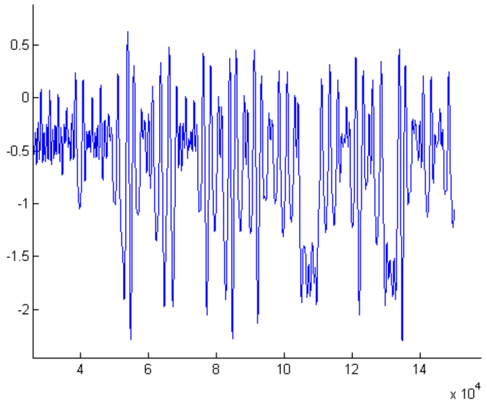

Figure 7. Measured voltage versus time (in 0.1ms) for a chaotic run at 2100 counts, 4Hz.

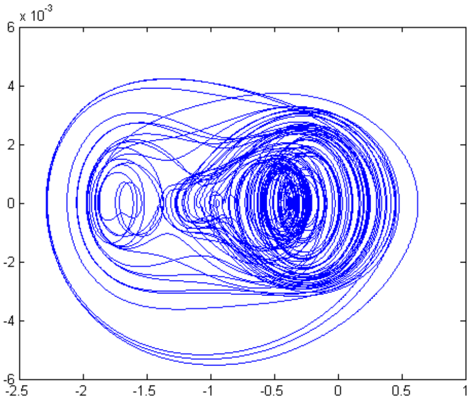

Figure 8. Phase portrait of $\dot{x}$ (V/s) vs. x (V) for a chaotic run at 2100 counts, 4Hz.

elliptical structure folded over on itself.

C. Attractor Reconstruction

The attractor for chaotic behavior was reconstructed using a time-delay embedding technique[7]. This technique plots $x(t)$ vs. $x(t+\tau)$ (or higher dimensional embeddings with offsets of integer multiples of τ), where τ is calculated to minimize the mutual information between the two dimensions. Figure 10 shows the results of this minimization process, which calculated an offset of 42.1ms. An alternative selection of embedding delay by finding the shortest time delay with autocorrelation between the axes near e^{-1} yielded a slightly longer 45.7ms, as shown in Figure 11. Since mutual information is considered a more robust method 42.1ms was used for attractor reconstruction.

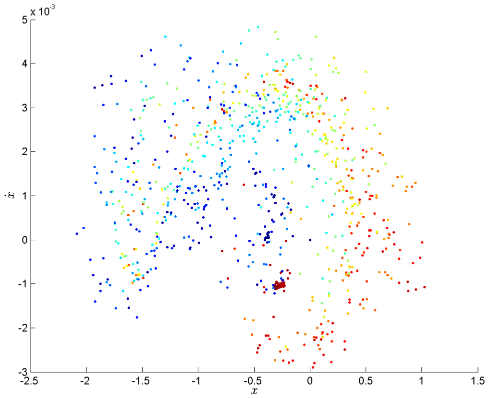

Figure 9. Recurrent Poincaré section at 4Hz of the phase portrait in Figure 8, with points colored according to their map sequential order.

Because of our prior belief about the dimensionality of the system, an embedding dimension of 3 was used. The 2-dimensional reconstruction is also shown in Figure 12 to give some insight into the form of the projection of the 3-dimensional reconstruction in Figure 13. In the 3D reconstruction, spirals to limit cycles near the potential wells form an

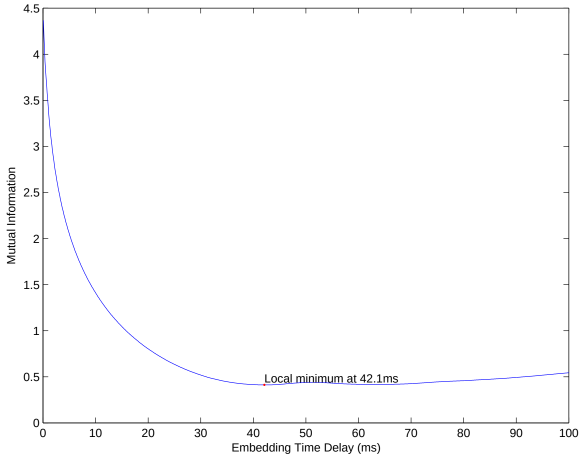

Figure 10. Mutual information minimization for 2-dimensional time delay embedding attractor reconstruction.

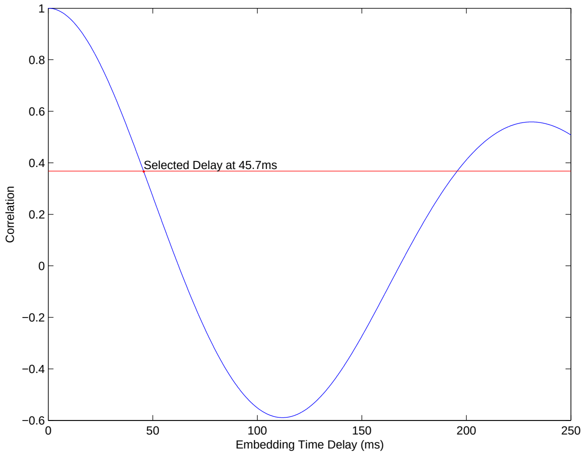

Figure 11. Autocorrelation selection for 2-dimensional time delay embedding attractor reconstruction.

hour-glass-like double funnel, with one funnel much larger than the other, reflecting the asymmetry of the system.

The largest Lyapunov exponent of the attractor was estimated from this 3D reconstruction using a nearest neighbors method[8]. Letting $d_j(k)$ denote the distance between the jth pair of nearest neighbors at time $i\Delta t$, we plot the line $y(k) = \frac{1}{\Delta t}\langle \ln d_j \rangle$, where $\langle \cdot \rangle$ is the average over j. The largest Lyapunov exponent is then given by the slope of the least squares fit to this line. This fit is shown in Figure 14. The estimated largest Lyapunov exponent for the reconstructed attractor was 0.0196; a positive value means nearby trajectories diverge exponentially quickly, a sufficient condition for chaos.

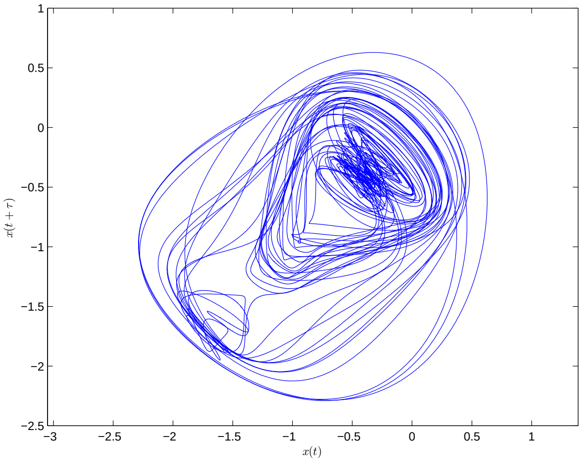

Figure 12. Attractor reconstruction of experimental data via 2D time delay embedding for $\tau = 42.1$ms.

IV. DISCUSSION

Though the asymmetric system demonstrated chaos at the forcing values calculated in the prior section, simulations of a symmetric system using this forcing and the parameters calculated in Table I resulted in either small f or large f limit cycles, as shown in

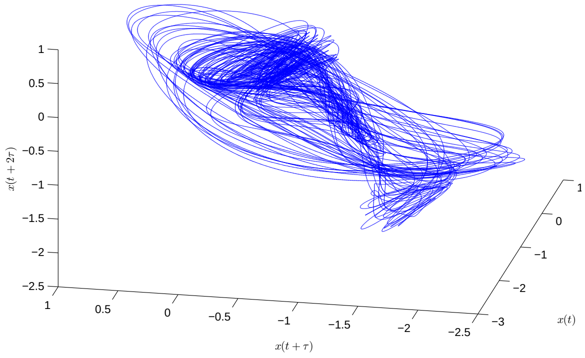

Figure 13. Attractor reconstruction of experimental data via 3D time delay embedding for $\tau = 42.1$ms.

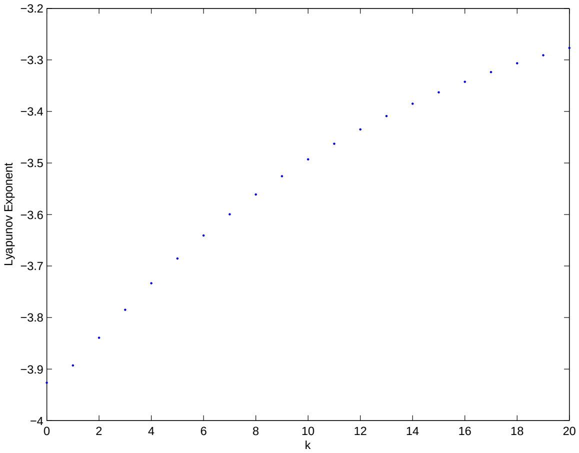

Figure 14. $\frac{1}{\Delta t}\langle \ln d_j(k) \rangle$ vs. k. The slope of the least-squares fit line gives us an estimate of the largest Lyapunov exponent, which is 0.0196 in this case.

Figures 15, 16, and 17. Therefore an asymmetric system can produce chaotic behavior even though a symmetrization of either of its potential wells would not. Since the left well parameters produce small f behavior and the right well parameters produce large f behavior, this is not surprising. However, an average of these estimates also produces large f behavior, indicating the likelihood of chaos of an asymmetric potential well can not be estimated through a simple average of the parameters of each of its wells.

The right well simulation did produce a brief chaotic transient before nearing the limit cycle, but this transient was much too brief to perform meaningful Poincaré sectioning, attractor reconstruction or Lyapunov exponent analysis for quantitative comparison with experimental data as we had hoped.

Though the Duffing oscillator and the mechanically forced double-well beam have been well studied, and promising approaches to address the issues encountered in these experiments with asymmetric potentials are in the literature[4,5], these experiments still provoke interesting research questions despite our original research goals not being met. There are questions of estimating asymmetric potentials from empirical data, and potential applications of computational and statistical learning techniques to this task. Our original questions regarding non-sinusoidal forcing are still applicable in the context of asymmetric potentials. But there is also the question of treating this is a diagnostic or controls problem: identifying empirically when mechanical systems are not responding as anticipated, either due to structural defects such as the asymmetric potential or through actu-

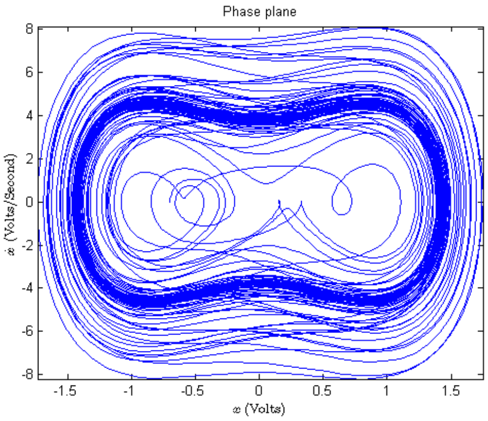

Figure 15. Phase portrait of a simulation starting form $(-0.7, 0)$ using parameters estimated from the left well. The system approaches the large f limit cycle.

ation inaccuracies such as failure of our motor to match our forcing signal. Though controls is a vast and well-studied field, there may be potential for crossover techniques from other domains, such as an episodic or batch learning rather than online models where unexpected potentials and actuations are identified during one trial, likely causes are abducted from the data, and forcing is adjusted for the next trial to approximate the idealized model.

ACKNOWLEDGMENTS

We would like to thank Dr. Daniel Goldman, Nick Gravish, Mark Kingsbury, Jeff Aguilar, Feifei Zhang, and the rest of the CRAB Lab for their expertise, time, and resources in completing this project.

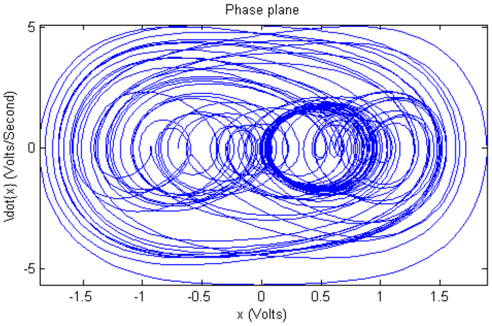

Figure 16. Phase portrait of a simulation starting form $(-0.7, 0)$ using parameters estimated from the right well. After a brief chaotic transient the system approaches the small f limit cycle.

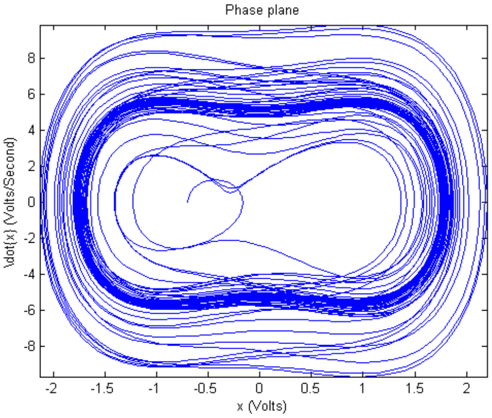

Figure 17. Phase portrait of a simulation starting form $(-0.7, 0)$ using parameters estimated from the average of both wells. The system approaches the large f limit cycle.

REFERENCES

[1] G. Duffing, *Erzwungene Schwingungen bei veränderlicher Eigenfrequenz und ihre tech-*

nische Bedeutung, 41-42 (F. Vieweg & sohn, 1918).

[2] F. Moon and P. Holmes, "A magnetoelastic strange attractor," Journal of Sound and Vibration **65**, 275–296 (1979).

[3] P. Holmes and P. Holmes, "A nonlinear oscillator with a strange attractor," Philosophical Transactions of the Royal Society of London. Series A, Mathematical and Physical Sciences **292**, 419–448 (1979).

[4] V. Chizhevsky and G. Giacomelli, "Experimental and theoretical study of vibrational resonance in a bistable system with asymmetry," Physical Review E **73**, 22103 (2006).

[5] S. Jeyakumari, V. Chinnathambi, S. Rajasekar, and M. Sanjuan, "Vibrational resonance in an asymmetric duffing oscillator," International Journal of Bifurcation and Chaos **21**, 275–286 (2011).

[6] J. Berger and G. Nunes Jr, "A mechanical duffing oscillator for the undergraduate laboratory," American Journal of Physics **65**, 841 (1997).

[7] A. Fraser and H. Swinney, "Independent coordinates for strange attractors from mutual information," Physical review A **33**, 1134 (1986).

[8] M. Rosenstein, J. Collins, and C. De Luca, "A practical method for calculating largest lyapunov exponents from small data sets," Physica D: Nonlinear Phenomena **65**, 117–134 (1993).